GNSS Indoors
Fighting the Fading
Part 1

GÜNTER HEIN, MATTEO PAONNI, VICTORIA KROPP, AND ANDREAS TEUBER

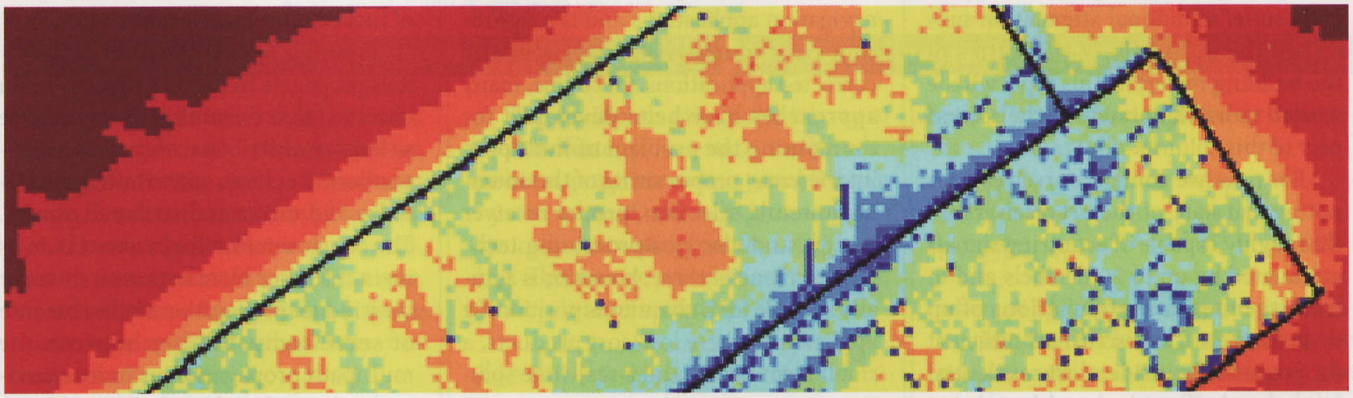

CNES

The ability to receive low-power GNSS signals inside buildings represents a veritable Holy Grail for product designers and manufacturers. Despite increases in receiver sensitivity and sophisticated signal-processing techniques, consistent and robust positioning indoors has yet to be achieved. In this first of a two-part exploration of the subject, the authors review existing models of indoor signal processing and the results of a new test designed to create an original model of satellite-navigation signal behavior as it propagates through diverse room shapes and building materials.

A common thesis expressed frequently in recent years asserts that GNSS does not work in indoor environments. Surely, however, this simplistic assumption is no longer tenable.

Receivers are becoming ever more sensitive due to ceaseless progress in chip technology and processing power. Moreover, with the advent of new GNSS systems under development, the number of available satellites and signals is expected to be considerably larger within a few years.

Unfortunately, high sensitivity is only one milestone on the road to success. The topic is more complex and processing GNSS positions indoors has a catch. In the vast majority of cases the navigation signal does not reach the receiver antenna via a direct line-of-sight, but rather experiences such phenomena as reflections, diffraction, or scattering when entering a building and propagating indoors.

We may summarize these effects with the term "fading." They typically lead to an extension of the estimated pseudorange and may result in severe deterioration of position accuracy.

In order to cope with these non-line-of-sight signals a laborious investigation of the indoor propagation channel is needed to provide a substantial understanding of the actual effects of this environment on GNSS signals.

This two-part column starts with an overview of existing channel models, examines new insights gathered from experiments that have recently been carried out, and presents a new satellite navigation–specific channel model. These activities shine a light on essential model parameters as well as construction materials of the building, shapes and contours of the environment, and incident angles of arriving signals. The second part of the series will apply these lessons learned to the Galileo signal itself.

Vision of Indoor Error Model

A GNSS user, roaming around outdoors in an area without buildings and obstacles, has no reasons to doubt the position solution that is displayed by his equipment, although many miles of the signal path pass through a medium other than vacuum. The ionosphere and the troposphere are the two relevant layers of the atmosphere that may affect a GNSS signal; indeed, these atmospheric layers cause nothing but fading.

For both the ionosphere and troposphere, researchers have developed powerful models in order to constrain the errors induced by them. As a matter of course, these models are implemented in every imaginable GNSS processing package.

Today, it might sound utopian, but should it not be possible to develop models that could similarly be applied to the fading induced by indoor measurements and include these routinely in GNSS signal-processing packages? In order to answer this question, we first ought to recount what makes the indoor channel so distinctive.

Signals propagating indoors apparently suffer additional attenuation subject to the permittivity properties of the building material. This topic will be treated more elaborately in the second part of this column.

For now, we content ourselves with noting that state-of-the-art receivers are thoroughly capable of acquiring signals attenuated by up to 20 decibels and to track them even at attenuations of up to 40 decibels. This, in turn, is sufficient for positioning inside most residential houses and office blocks, although not in underground car parks and cellars.

Indoor versus Outdoor

Despite all atmospheric effects, the direct path between the satellite and an outdoor receiver with unlimited view to the sky is called the line-of-sight (LOS). Indoors, however, a LOS is hardly in evidence, because the signal path undergoes the fading phenomena mentioned earlier. These kinds of signal paths are referred to as non-line-of-sight (NLOS).

In the outdoor channel case, NLOS is also well-known due to obstacles that may reflect the signal before it reaches a receiver's antenna. However, outdoors the NLOS signal is usually delayed, arriving behind the LOS signal, and of a smaller amplitude. An indoor user has to cope with an NLOS signal that may well be the first and strongest one.

Apart from this geometrical consideration, we can also consider the matter from the viewpoint of electrical engineering. A GNSS signal received indoors by a user's equipment is different from the one transmitted by the satellite. Interactions with the building material or electric power lines distort the signal.

The distortions that the RF signal experiences also result in the fading and multipath. *Fading* is the fluctuation of the signal amplitude. *Multipath* is the appearance of NLOS signals at the receiver antenna with a sufficiently short delay that it leads to an undesired distortion of the autocorrelation function during signal processing and, hence, to an extended pseudorange estimation.

Multipath is certainly the dominant error source in high precision satellite navigation applications and is a significant error source in non-differentially corrected applications. Of course, many approaches have been developed for overcoming the problem of multipath interference: proper siting of the antenna, antenna selection, proper receiver design, and also postprocessing techniques. None of these, however, is actually suitable for a ubiquitous positioning application where low-cost products, a small form factor, and a real-time solution are most important.

Multipath properties are different for indoor and outdoor environments. In the outdoor case, the maximum excess delay can raise values up to 100 microseconds for reflections from very distant objects (hills, city skylines, etc.), whereas in the indoor environment it is limited to about 1 microsecond. Furthermore, the relevant sources of outdoor multipath are fixed objects. In contrast, the indoor case may include moving people, which can annihilate the temporally stationary properties of the channel.

Another important difference between indoor and outdoor signal processing is the possible Doppler shift. For a lot of outdoor applications rapid motions and high velocities of the user result in a considerable Doppler shift, which can be detected and used in positioning solutions. However, for most of the indoor applications the Doppler shift caused by the user's velocity is negligible, which facilitates the acquisition process that is already sufficiently complicated in indoor environments.

In any case, all the applications related to satellite navigation would benefit from an instrument that can describe this complicated transmission channel as accurately as possible. To help accomplish this, a suitable statistical model is a cornerstone for describing the behaviour of the channel under diverse conditions.

Finding a Starting Point

Historically, the foundation of the work on indoor multipath propagation was provided by George L. Turin in research focusing on an urban environment. (See Additional Resources section at the end of this column for relevant references.)

Looking to how the multipath signals propagate in urban canyons, Turin observed that the multipath rays arrive as Poisson-distributed events with independent Rayleigh-distributed amplitudes and uniform distributed phases. The conclusions of Turin were taken as main reference by many researchers for their indoor propagation studies because of some comparability between the multipath propagation in indoor environments and in the urban canyons, as shown in a paper from H. Hashemi cited in the Additional Resources.

In 1987 Saleh and Valenzuela presented the first model specifically dedicated to signal propagation in an indoor environment (see the Additional Resources). The main novelty of this work was that Saleh and Valenzuela observed in their data that the multipath rays arrive at the receiver grouped in clusters.

This model relies on previous work of Turin but, maintaining the approximation that multipath rays arrive at the receiver according to a Poisson process, they introduced a second Poisson process to describe the clusters' times of arrival.

After 20 years the Saleh and Valenzuela (S-V) model still represents the fundamental reference for anybody who wants to deal with the problem of the channel modelling in an indoor environment. The details of the model are presented in the following section. In any case, readers should be aware that this model was dedicated to RF signal propagation in general, and not to satellite navigation in particular.

The Saleh-Valenzuela Model

The S-V model starts with the physical realization that rays arrive in clusters:

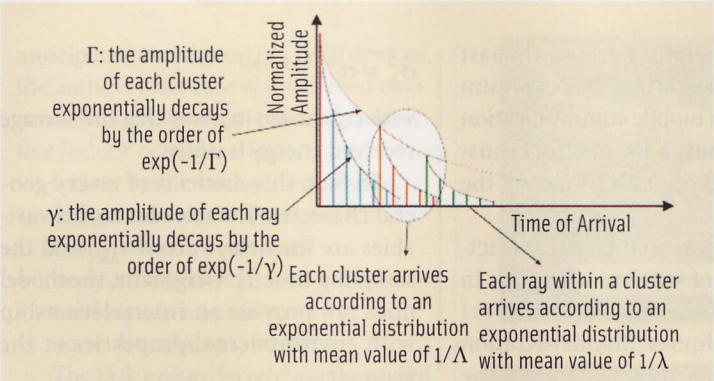

FIGURE 1 Saleh-Valenzuela Power Delay Profile Model

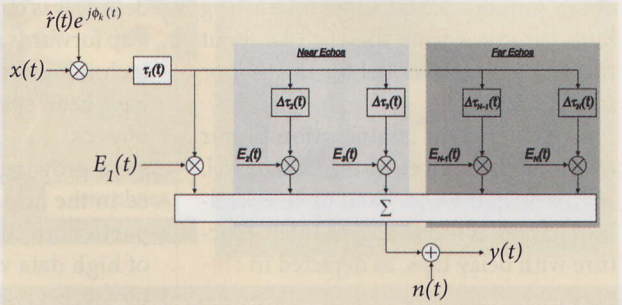

FIGURE 2 The filter structure with delay taps of the Lutz Model

one or more packages of signals with different lengths within the observation window. Not all the clusters or packages of signals are of the same amplitude. In fact, the subsequent clusters are attenuated in amplitude after the first one. Moreover, the arrivals within a single cluster have amplitudes that decay over time at various rates.

The S-V model proposes that both of these decaying patterns, namely that associated to a particular cluster and that within the cluster, follow an exponential function of time, and are controlled by two time constants: Γ, the cluster arrival decay time constant, and γ, the ray arrival decay time constant, as depicted in **Figure 1**.

The Saleh–Valenzuela multipath model is given by the discrete time impulse response:

$$h_{discrete}(t) = \sum_{l=0}^{\infty} \sum_{k=0}^{\infty} \beta_{kl} e^{j\phi_{kl}} \delta(t - T_l - \tau_{kl}) \quad 1$$

where:

- l represents the clusters and k represents the different multipath components arrivals within each cluster
- β_{kl} is the multipath gain coefficient of the kth multipath component (MPC) in the lth cluster
- $e^{j\phi_{kl}}$ term represents a statistically independent random phase associated with each arrival, where ϕ_{kl} is uniformly distributed within $[0,2\pi)$
- $\delta(\cdot)$ is the Dirac function
- T_l is the delay of the lth cluster
- τ_{kl} denotes the kth path arrival delay with respect to the first arriving MPC in the lth cluster. The number of clusters and MPCs may theoretically extend over infinite time.

The multipath gain of the kth ray of the lth cluster β_{kl} is a statistically independent, positive random variable mean square value of which $\{\beta_{kl}^2\}$ is a monotonically decreasing function of $\{T_l\}$ and $\{\tau_{kl}\}$. The average power at a given delay, $T_l + \tau_{kl}$, is represented by

$$\overline{\beta_{kl}^2} = \overline{\beta^2(T_l, \tau_{kl})} = \overline{\beta^2(0,0)} \cdot e^{-T_l/\Gamma} \cdot e^{-\tau_{kl}/\gamma} \quad 2$$

where $\overline{\beta^2(0,0)} = \overline{\beta_{00}^2}$ is the average power gain of the first ray of the first cluster.

With respect to Γ and γ, they are, as mentioned earlier, the power-decay time constants of the clusters and of the rays, respectively.

In the work of Saleh and Valenzuela the amplitude of each arrival is assumed to be a Rayleigh-distributed random variable whose mean square value is described by a the double-exponential decay.

A work from R. Jean-Marc Cramer (see Additional Resources) underlines the fact that the cluster power-decay factor is strongly related to the architecture of the building, while the ray power-decay factor is dependent on objects that are close to the receiver, such as the furniture of the particular room in which the measurements are performed.

The time of arrival (TOA) of the lth cluster is denoted by T_l, with $l = 0,1,2, \ldots$, while the TOA of the kth ray, measured from the beginning of the lth cluster, is denoted by τ_{kl}, with $k = 0,1,2\ldots$. For the first cluster $T_0 = 0$, and for the first ray within the lth cluster, $\tau_{0l} = 0$.

According to the S-V model, T_l and τ_{kl} are controlled by two independent Poisson processes described by the inter-arrival exponential probability density-functions, as follows:

$$p(T_l | T_{l-1}) = \Lambda \cdot e^{-\Lambda(T_l - T_{l-1})}, \; l > 0 \quad 3$$

$$p(\tau_{k,l} | \tau_{(k-1),l}) = \lambda \cdot e^{-\lambda(\tau_{k,l} - \tau_{(k-1),l})}, \; k > 0 \quad 4$$

where $p(T_l|T_{l-1})$ represents the probability that the lth cluster arrives after the previous one has arrived. Likewise, the $p(\tau_{k,l}|\tau_{(k-1),l})$ represents the probability that a ray within the lth cluster arrives after the previous $(k\text{-}1)$ ray has arrived. Each cluster consists of many paths, and therefore, as a result, $\lambda > \Lambda$.

Saleh and Valenzuela explain that the first cluster that arrives at the receiver is formed by the transmitted wave following a more-or-less "direct" path to the receiver. This "direct" path is not necessarily a straight line, which, in fact, appears infrequently in the indoor environment, but it is a "simple" path, that does not go through "too many" walls.

Bringing the Outdoor Channel Model Indoors

As has been pointed out by B. W. Parkinson (see Additional Resources) *"on its transmission path from a satellite to a navigation receiver the signal suffers attenuation, reflections and phase rotations due to building, trees and other obstacles."*

Several statistical models for the mobile satellite channel exist in the literature, such as the Loo model, the Nakagami model, the Norton model, or the Lutz model. In the Additional Resources the interested reader can find some references about all these works.

All these models take on the problem of estimating the behavior of the mobile

satellite channel in evaluating the case of an "outdoor" user. Some interesting hints can come from these works about the way to find a model for the indoor satellite channel.

An important contribution to our efforts has been given by the Lutz model. In this work the wideband mobile satellite channel is modeled as a filter structure with delay taps, as depicted in **Figure 2**.

As explained by Lutz et alia, the complex impulse response $h(t, \tau)$ of the satellite wideband channel can be superimposed to a sum of N signal paths with amplitudes $E_k(t)$ and delays

$$\tau_k(t)=\tau_1(t)+\Delta\tau_k(t),\ k=2...N \quad (5)$$

Then the total complex impulse response can be expressed as follows:

$$h(\tau,t)=\sum_{k=1}^{N} E_k(t)\cdot\delta(\tau-\tau_k(y)) \quad (6)$$

and the amplitude of each echo is complex and can be expressed by:

$$E_k(t)=a_k(t)\cdot e^{j\phi_k(t)} \quad (7)$$

The different taps of the filter of Figure 2 are classified; specifically, the channel impulse response with N echoes can be divided into three parts with different behavior: direct path, near echoes, and far echoes with a statistical characterization given for each part.

The model parameters that describe the statistical characteristics of all these components are then presented in a table showing the results of varying the elevation of the transmitting satellite.

Because the behavior of the satellite channel – regardless of whether indoor or outdoor – is strongly influenced by the relative positions of the satellite that is transmitting the signal and the user equipment receiving it, we will keep the approach followed by Lutz in mind. Later on, we will try to verify whether such an idea could be applied to the indoor case, too.

Consulting the Specialists

Before taking up the behavior of the satellite channel, we first would like to pay the indoor communication specialists a flying visit. We are convinced that this might be helpful because the last decade was characterized by a quantum leap forwards in mobile communication technology. Thus, a lot of effort must have been spent on understanding the physics.

A growing potential is still predicted in the fields of wireless networks, in particular considering the transport of high data volumes. Standardization of the PHY/MAC layer is a big issue closely connected with the industrial support and, consequently, the market opportunities.

For wireless networks the most important global standards have been defined by the joint working groups of IEEE 802. To mention some of the recently most active efforts, there are standards 802.11 for WLAN, 802.15 for WPAN, and 802.16 for WiMAX.

The formulation of these standards is founded on a comprehensive consideration of all relevant physical aspects comprising the propagation channel. Essential additional contributions from outside the IEEE working groups complete the marvellous "offer" on the range of indoor channel models. Representatively, we will consider channel model developments for IEEE 802.11 (WLAN), an alternative WLAN approach dedicated to large office environments, and for ultra-wideband communications according to IEEE 802.15.

A WLAN Channel Model

The channel model associated with WLAN technology is of relatively low complexity compared to the ultra-wideband channel model. Its underlying idea is the "tap delay line" (TDL), which asserts that the signal portions do not arrive at once, but in subsequent taps caused by multipath. The power of the taps is exponentially decaying, whereas the fading of each individual tap statistically follows a Rayleigh shape.

The TDL model assumes that each of the channel taps is drawn from an independent complex Gaussian random variable with an average power profile that decays exponentially. The energy of each channel tap k is given by

$$\sigma_k^2=\sigma_0^2 e^{-kT_s/\tau_{RMS}}$$

with σ_0^2 chosen in a way that the average received energy is unity.

In fact, this model is of a very general character. The relevant model variables are the delay spread τ_{RMS} and the sampling time T_S. Originally, the model does not provide an interrelationship with environmental properties or the geometry.

Linking EM, Acoustics

Bach Andersen et alia have tried to link electromagnetic properties with acoustic properties and applied the reverberation theory (see Additional Resources). Studying cumulative power distributions to wireless access points of different indoor locations, they found two characteristics. Locations close to the access points show Ricean distributions and locations farther away show Rayleigh distributions whose associated power delay profiles demonstrate a strict logarithmic decay as soon as the delay exceeds a certain value.

These authors propose to follow the tap delay line model for all propagation paths shorter than a threshold that they call the *reverberation distance*. This distance primarily depends on the size of the room and the average absorption coefficient of the walls.

For propagation paths that extend beyond the reverberation distance, the diffuse field adopted from acoustics that is characterized by a simple exponential decay can sufficiently well describe the indoor channel.

Comprehensive UWB Model

The extensive activities of the IEEE task groups on ultra-wideband (UWB) did consider channel models. One of the task groups (802.15.4a) even published three different models – two UWB models for various frequency ranges and one narrowband model for the frequency range around 1 MHz.

For the two ultra-wideband models the 802.15.4a task group described a generic channel model structure. The two models differ only in terms of parameterization. Keeping in mind the

anticipated circulation of UWB devices, the authors took care of diversified environments that even go beyond a restrictive indoor consideration:

- indoor residential environments
- indoor office environments
- industrial environments
- body-area networks
- outdoor environments
- agricultural areas, farms.

The task group derived an associated group of parameters for each of the six environments. The basic characteristics of the UWB generic model focus on the channel only and intentionally blank out antenna effects.

The parameterization can be divided into three subgroups: parameters describing the pathloss, parameters describing the power delay profile, and parameters deriving small-scale fading.

The model proposes an exponential law and frequency dependency for the pathloss. Moreover, the Saleh-Valenzuela power delay profile model was subjected to some modifications, such as possible delay dependence of cluster decay times.

For dedicated NLOS environments the general shapes of the power delay profiles might change in a way that they first increase before they decrease again. The small-scale fading follows a Nakagami distribution. The list of parameters that vary with the previously mentioned environments is rather long:

Subgroup 1: Parameters subject to pathloss:

- pathloss exponent
- shadowing standard deviation
- frequency dependence of the pathloss

Subgroup 2: Parameters subject to power delay profile

following Saleh-Valenzuela:

- mean number of clusters
- cluster arrival rate
- ray arrival rates
- cluster decay constant
- ray decay constant

following the alternative shape

- power delay profile increase to local maximum
- power delay profile decay afterwards
- attenuation of the first component

Subgroup 3: Parameters subject to small-scale fading:

- cluster shadowing variance
- Nakagami m factor for first component, mean, and variance

Specifying the parameters for the different environments and the two frequency ranges would go beyond the scope of this article. Due to the attempt to be as general as possible, the model becomes bulky to some extent.

The three channel models might be sufficient to give the reader an idea on the diversity of the approaches, in which signal factors including the frequency range and the bandwidth, as well the shape of the environment, serve as key criteria.

We have learned a lot from this review of existing outdoor and indoor models. All the indoor models have in common the expectation that the signal source as well as the receiver are indoors. They are also not direction-dependent.

In contrast to these assumptions, a dedicated satellite-navigation channel model has to put major effort onto these points. As a result, we become more and more convinced that we have to develop something new.

Conducting a Field Campaign

The existing models can already serve as a guideline for us, for example, with respect to data acquisition techniques and the tools to be applied for the development of the model.

The drawbacks of the existing models provoked us to carry out a new field campaign applying L-band frequencies and a measurement set-up that takes into consideration the varying elevations and azimuths of the transmitter, which represents the GNSS satellite signal source.

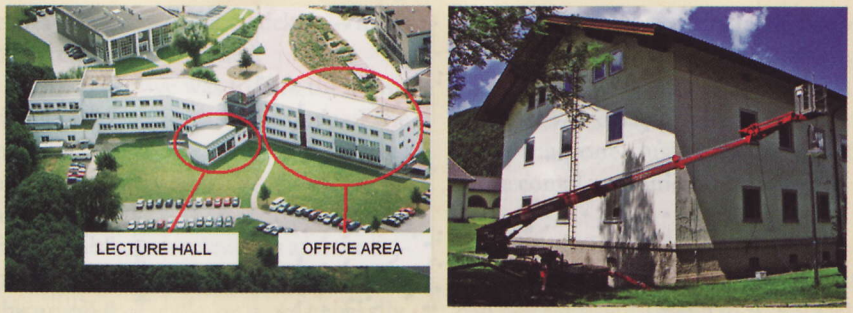

FIGURE 3 Buildings in which field tests were conducted; the channel sounder transmitter antenna was located in the cage on the end of the crane in the right-hand photo.

This campaign considered two different buildings as well as two different room shapes. Most of the data was captured in a typical office building at IMST GmbH in Kamp-Lintfort (North Rhine-Westphalia) constructed of a concrete frame with sand-lime brick outer walls, concrete floors/ceilings, and light-weight inner walls. (See **Figure 3**, left, office area.)

In order to cover many azimuth/elevation combinations for the transmitter location, a mobile crane was used so that the transmit antenna could be placed at different heights in front of the building facade. To accomplish the variation of the azimuth, six different transmitter positions were defined along the facade of the building.

The receiving antenna positions of the channel sounder in the rooms of the office area were on profiles perpendicular to the wall with distances of zero, two, and four meters from the wall. The effective azimuth and elevation combinations that have been covered by the measurements can be seen in **Figure 4**.

The measurements have been performed using a RUSK SX channel sounder modified and operated by the company IMST GmbH. The merit of a channel sounder is the chirp signal that it transmits providing an almost flat amplitude of the spectrum over its nominal bandwidth of 120 MHz. Thus, the signal-to-noise ratio is equal for the whole bandwidth.

The chirp length is 6.8 microseconds, representing a maximum observ-

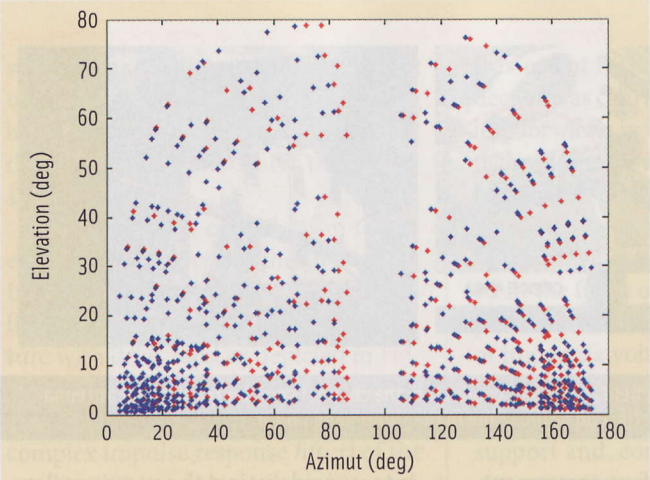

FIGURE 4 Distribution of azimuths and elevations during test campaign

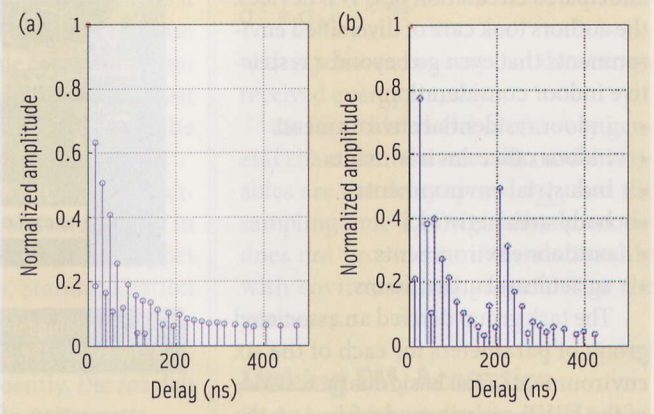

FIGURE 5 Power Delay Profiles – Scenario 1 and Scenario 2

able delay of about two kilometers. For the indoor channel characterized by short delays, the delay resolution of 8.3 nanoseconds (= 2.5 meters) is of higher importance.

Other key technical specifications of the channel sounder include its transmitting power of -34 dBm EIRP, the receiving sensitivity of -90 dBm, and the instantaneous dynamic range of the receiver of 30 dB.

The single time-domain impulse response of the channel sounder is equivalent to a set of samples of the corresponding (frequency domain) transfer function $S_{21}(f)$ of the radio channel at given frequencies:

$$H(n) = S_{21}(f(n)), n = 1,..., N \quad (8)$$

where $f(n) = 1625\ MHz + (n\text{-}1) * df$. n is the frequency index running up to $N = 1{,}024$ responsible for the incrementing of the frequency by $df = 146484.375$ Hz. S_{21} is the conventional denotation for transmission coefficients in contrast to, e.g., S_{11}, denoting reflection phenomena.

The center frequency of 1700 MHz does not match exactly with one of the Galileo frequencies and had to be chosen due to technical constraints. However, it is well located within the L-band.

For statistical reasons and in order to overcome locally generated fading effects (e.g., fading caused by furniture), a total number of 256 channel impulse responses have been generated for each point. Moreover, the receiving antenna was not fixed, but slowly moved around the nominal test site.

Pre-Processing the Channel Sounder Data

A rectangular signal in the frequency domain leads to a sinc function in the time domain that possesses a number of side lobes, which might cover weaker echoes of adjacent signals. In order to reduce this effect, we have to apply a window function and then carry out the normalization with respect to bandwidth.

To describe a channel that consists of several superimposed independent paths, we used the Turin Model. The fundamental expression of the Turin model can be given as:

$$H(f) = \sum_k S_k \exp(-j2\pi f\tau_k) \quad (9)$$

where S_k and τ_k are the complex gain and delay of path k.

This model represents a parametric model of the power delay profiles. In it, the estimated parameters $\{(\hat{s}_k, \tau_k)\}$ have been determined. We accomplished this using an iterative method to minimize the relative model error energy.

Instead of using some error threshold criteria to halt the iteration, which may result in a different number of paths for each measurement, a fixed number of 150 paths was extracted from each measurement. In the subsequent processing steps these 150 paths have to be reduced to a reasonable number using a powerful mixture of software routines and visual anticipation.

Automation of Data Analysis

The whole data analysis proved to be a good compromise between automatized routines and visual inspection. The first steps of the data analysis were subjected to automation, as follows:

- For each power delay profile, the delay and the amplitude values of all the signals have been normalized to the delay and amplitude of the strongest path. This allows comparison of the different power delay profiles within them.
- After that, looking to the physical dimension of the building in which the measurements have been performed, the maximal excess delay has been set to 500 nanoseconds.
- A threshold of 40 decibels has been applied to the power delay profiles. This means that all the reflections with power levels 40 dB or more below the power level of the direct path have been excluded from our analyses. We selected the value of the threshold taking into account that signals that are 40 dB or more weaker than the strongest one are, in principle, not detectable by common receivers as the cross-correlation provided by the codes will not provide isolation levels higher than 40 dB.

Plus Visual Inspection

The second step required visual considerations. The goal was to look for some general characteristics of the data. We

soon identified two well-defined groups of power delay profiles:

- The first group consisted of smoothed power delay profiles. An example of a power delay profile belonging to this group is depicted in Figure 5-left. This group of measurements has been designated as SCENARIO 1.
- The second group of measurements consisted of power delay profiles with a more complicated shape, in which a "grouped" structure of the signal was evident. Figure 5-right depicts an example of a power delay profile belonging to this group of measurements, named SCENARIO 2.

Cross-Linking Power Delay Profiles with Geometry

Paying attention to the first scenario, we should recognize that the measurements were taken close to the wall and have a low elevation and azimuth of the transmitter with respect to the receiver. On the other hand, the measurements belonging to the second group were almost all taken far away from the wall, with high values of the transmitter's azimuth and elevation.

We should underline that *"elevation"* means the transmitter's absolute elevation in degrees above the floor, while *"azimuth"* is a relative angle defined by means of a given reference plane, as depicted in Figure 6.

Almost all the measurements that belong to the first scenario had only one wall between the transmitter and the receiver, while in the second case — characterized by grouped delays — more than one wall intervened.

Our objective was to link these two different cases to the geometry of the path between transmitter and receiver and, as a consequence, to the elevation and the azimuth of the transmitter. In fact, increasing the elevation and the azimuth of the transmitter also increases the number of walls, or more generally, the "complexity" of the path, through which the signal has to travel.

What Can the Saleh-Valenzuela Model Offer?

In this context, the Saleh-Valenzuela model seemed to be particularly suitable for describing the measured data. The clustering phenomenon (discussed earlier and illustrated in Figure 1) seems to describe the "grouped" structure observed in our tests very well. Furthermore, the number of clusters seems to depend on the building superstructure.

In fact, the following propositions of the S-V model have been confirmed by the actual observations:

- Each cluster has attenuated amplitude in comparison with the previous one.
- The signals that come within each cluster seem to decay with an exponential law.

So, without doubt the S-V model can act as a good baseline for the new model. No doubt, too, that some modifications to the model are still essential.

The power delay profiles of SCENARIO 1 — by virtue of the fact that few hindrances to the signal exist — present simply almost one cluster. However, when the signal propagates through more than one wall, as in SCENARIO 2, the power delay profiles appear with more than one cluster, as a result of a more complex geometry.

Geometry Sub-Scenarios

Sites with low elevation and low azimuth can certainly be assigned to SCENARIO 1 and those with high elevation and high azimuth, to SCENARIO 2. The clear distinction with respect to the shape of the power delay profiles encouraged us to subdivide the two scenarios further.

Thus, considering the available data volume, we found it reasonable to divide both azimuth and elevation values into 5 different bins: 10°, 25°, 40°, 60° and 80° for the azimuth and 10°, 15°, 30°, 50° and 70° for the elevation, respectively. In this way, we established 25 different sub-scenarios (See Figure 7). Through this new definition of sub-scenarios, we obtained a comprehensive description of the signal propagation environment.

Our next task was to conduct the parameter extraction for each group of measurements. On the one hand, the propositions of the S-V model have been proven to provide a suitable approach for our research efforts. On the other hand, a strong suspicion arises that the shape of the power delay profiles depends on geometrical parameters that made us refine the grain size of the scenarios.

Now the time has come to check whether this approach is fruitful.

We first assigned each available power delay profile to its corresponding

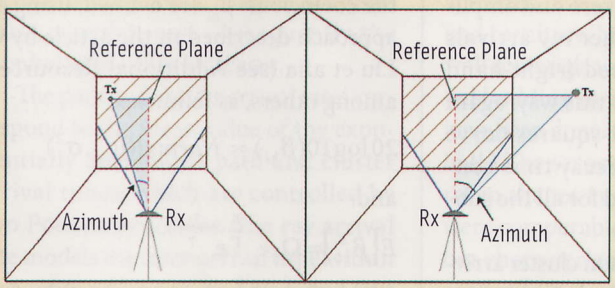

FIGURE 6 Definition of the relative azimuth for scenario 1 (left) and scenario 2 (right)

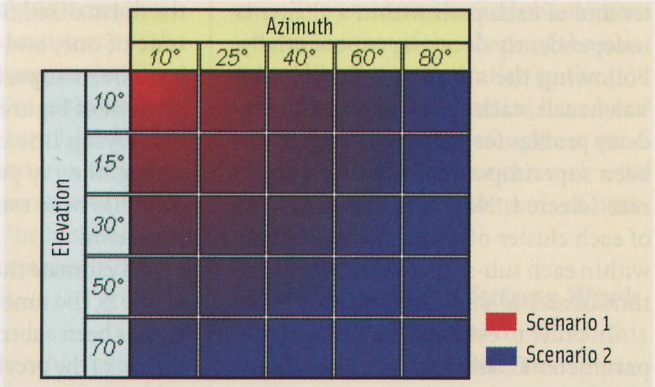

FIGURE 7 Scenarios subdivision into azimuth and elevation

sub-scenario. After the entire number of the 25 sub-scenarios was filled with the corresponding power delay profiles, we could extract the appropriate parameters of the S-V-model and observe whether or not the model parameters actually show a significant dependency with respect to the properties of the sub-scenarios.

To do this, we first had to find the number of clusters and the times of arrival of each cluster for each power delay profile. As stated earlier, the TOA of each cluster is the TOA of the first signal of the cluster. Finding a robust algorithm for the automatic identification of cluster regions is very difficult (see the article by A. F. Molisch et alia).

Therefore, following the most frequently used approach in the literature, (cfr. the articles by A. Saleh and R. Valenzuela, Q. H. Spencer et alia, and A. F. Molisch et alia), we selected the cluster regions manually by visual inspection and identified their TOAs. **Figure 8** shows an example of cluster selection.

In the second step, each path of the power delay profiles has to be assigned to a given cluster. As can be seen in Figure 8, two consecutive clusters can overlap. Therefore, to exactly determine each path of the clusters, the overlapping clusters have to be solved, which was done automatically using software developed for this purpose.

An example of application of this software is represented in Figure 8. In the figure, the first path of each cluster is coloured in red, and different clusters are represented with various colors.

As explained in the first part of this column, the amplitude of each cluster and of each path within a cluster is independently decaying exponentially. Following the approach of Saleh and Valenzuela, each cluster of all the power delay profiles for each sub-scenario has been superimposed and a mean decay rate selected. Note that the first path of each cluster of all the measurements within each sub-scenario represents the time of arrival of the entire cluster.

In order to estimate the cluster decay parameter Γ, all first paths have been superimposed and plotted on a semi-logarithmic plot. The estimation of Γ was

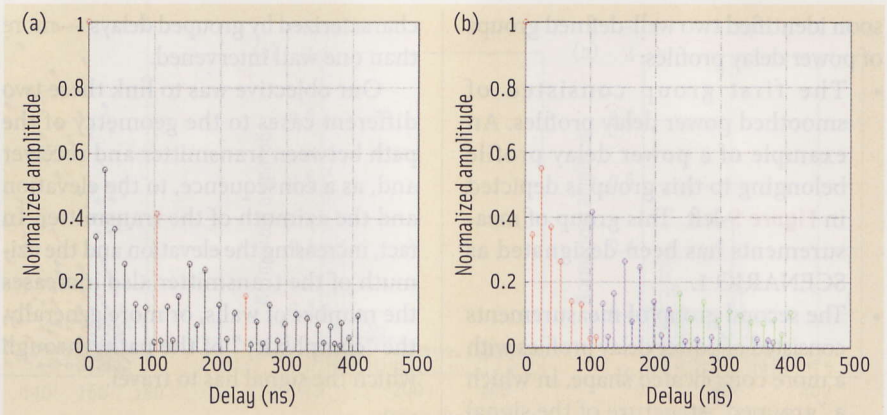

FIGURE 8 Cluster selection and overlapping cluster solution

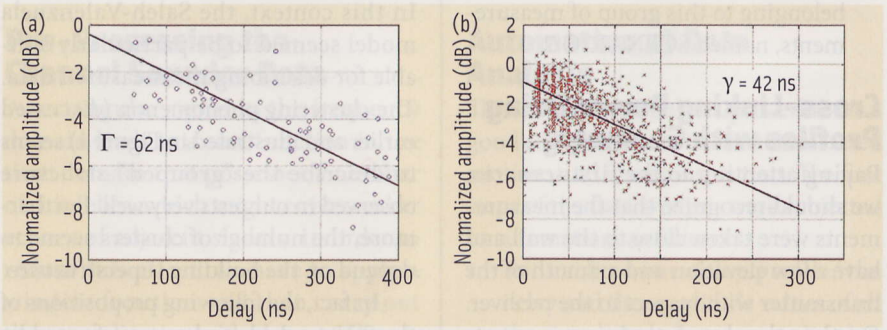

FIGURE 9 Ray and cluster decay time constant estimation: 80° azimuth, 15° elevation

found by inverting the negative slopes of a linear least squares curve fitting in the logarithmic plot. An example of the estimation of Γ is depicted in the left-hand portion of **Figure 9**, which belongs to the sub-scenario with 80 degrees of azimuth and 15 degrees of elevation. In this particular case the estimated value for the cluster power-decay time constant is 62 nanoseconds.

Similarly, in order to estimate the ray decay time constant γ, the first arrival of each cluster has been set to the normalized time of zero and amplitude of one, and all other ray arrivals have been superimposed (right-hand portion of Figure 9). In this way, again employing linear least-squares curve fitting, the ray power-decay time constant has been estimated for all the sub-scenarios.

To estimate the Poisson cluster arrival rate Λ, the time of arrival of each cluster has been subtracted from the time of arrival of the previous one. We estimated Λ by fitting the sample probability density function to the corresponding probability for each bin. The fitting has been done using a least mean square criterion. The same steps have been used also for the estimation of the second Poisson parameter, the ray arrival rate λ.

It has been observed that the lognormal distribution for the multipath gain magnitude results in the best fit to the data. Recalling the discrete time impulse response of the S-V model

$$h_{discrete}(t) = \sum_{l=0}^{\infty} \sum_{k=0}^{\infty} \beta_{kl} e^{j\phi_{kl}} \delta(t - T_l - \tau_{kl}) \quad (10)$$

the coefficients β_{kl} are defined, using an approach described in the article by C. Liu et alia (see Additional Resources) among others, as follows:

$$20\log10(\beta_{kl}) \propto Normal(\mu_{kl}, \sigma^2) \quad (11)$$

and:

$$E\left[\beta_{kl}^2\right] = \Omega_0 e^{-\frac{T_l}{\Gamma}} e^{-\frac{\tau_{kl}}{\gamma}} \quad (12)$$

where Ω_0 is the mean power of the first path of the first cluster, which in our case is equal to 1, and T_l and τ_{kl} are the time of arrival of the given cluster and ray, respectively. Using a least mean square

criterion, we estimated the σ^2 for each group of measurements.

We then calculated the mean value μ_{kl} for each path as seen in the work from C. Liu et alia, as follows:

$$\mu_{kl} = \frac{10\ln(\Omega_0) - 10T_l/\Gamma - 10\tau_{kl}/\gamma}{\ln(10)} - \frac{\sigma^2 \ln(10)}{20} \quad (13)$$

Relation between extracted parameters and geometry

We subdivided the model parameters into 25 different scenarios, depending on elevation and azimuth of the transmitter. Without listing all the extracted parameters — the values of which are probably not interesting for the reader — we want to give here some considerations on the obtained results. In particular, we are mainly interested in how the parameters change by changing the geometry, or in other terms, by varying azimuth and elevation.

As we have already somewhat extensively discussed, the clusters result from reflections, scattering, and diffraction due to the building superstructure. Our first results indicate that the mean number of clusters increases with increasing elevation and azimuth.

For example, a mean number of clusters with a value close to 1.0 has been found for the measurements taken at 10 degrees of azimuth and elevation of the transmitter, while a mean number of clusters 3.4 has been observed for the measurements taken at 80 degrees of azimuth and 70 degrees of elevation. This is due to the fact that for high values of elevation or azimuth, as we had speculated, the paths' propagation from the transmitter to the receiver becomes more complex, and consequently the number of clusters increases.

The path and cluster arrival rates correspond to the mean value of the exponentially distributed path and cluster arrival times, which are controlled by two Poisson processes. The ray arrival rate models the inter-arrival time within two consecutive rays, and we found that increasing azimuth or elevation decreases the mean inter-arrival time. With respect to the cluster arrival rate, it increases with the azimuth and elevation.

In regard to the power decay constants, we observed that they are also linked with the values of the azimuth and elevation. In fact, with increasing azimuth or elevation, the cluster power–decay constant increases while the ray power–decay constant becomes lower.

In **Figure 10** an intuitive summary of the observed relations between azimuth and elevation and the model parameters is depicted. As a first conclusion we can say that the original hypothesis of a link between the parameters of the model and the elevation and azimuth has been verified. Indeed, the mean number of clusters increases with the azimuth and elevation, and all the other parameters of the model also change by increasing the azimuth and elevation based on a constant principle.

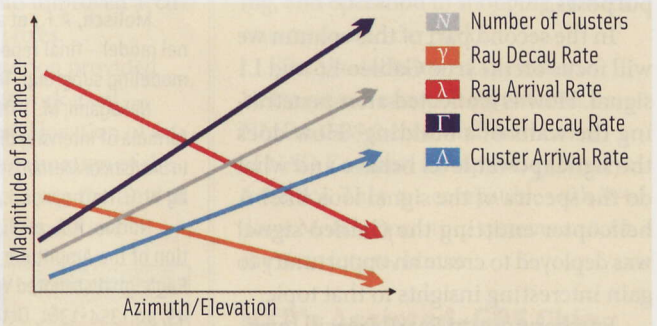

FIGURE 10 Model parameters versus satellite azimuth and elevation

Scouting Other Buildings

We are absolutely interested in verifying whether the parameters that have been extracted in a given building with certain characteristics can also be used to model another building characterized by different structure or different materials.

To test this premise, we extracted the model parameters in two new indoor environments with peculiar characteristics. The first test environment was characterized by a completely different shape and furniture, but the consistency of the wall materials was the same as the original building in which the main analysis have been done. (See Figure 3, left lecture hall.) The second test environment had room shapes and a superstructure that were comparable with the first building but characterized by completely different building materials. (See Figure 3, right.)

The results that were achieved in the first environment were confirmed in the two new environments: The parameters of our model change with the same ordered law with respect to the azimuth and elevation of the transmitter, as previously explained.

Moreover, comparing the results obtained in the two test environments with the original model parameters extracted in our analysis of the first building produced some interesting observations. First, the mean number of clusters remains almost the same. Actually, in all the three buildings, we discovered a very similar value for the number of clusters for the same values of azimuth and elevations.

This is a very important observation that surely needs to be verified with more accurate measurements, but it seems to bring an important first conclusion: using the azimuth and elevation of the transmitter, an initial estimation of the number of clusters can be done generally, not taking into account the building materials or superstructure.

Next, hanging the materials of the building, but maintaining constant its superstructure leads to model parameters that are very similar to the original ones. Therefore, as a second observation, we can say that if the shape of the considered building is similar to the one from which the parameters have been extracted, the model can give a good estimation of the indoor channel, with good capabilities also in terms of "generality".

Conclusions and Future Work

The amount of the data on which this work is based was moderate, in particular with respect to the diversity of architectural styles. For this reason we

think that future investigations have to be done to confirm and enhance the results presented here. More extensive field campaigns are necessary to estimate the model parameters accurately.

Furthermore, a proper investigation of additional indoor environments will allow a better understanding of the relationship between the various model parameters. In any case, the results that have been presented here clearly show that the elevation and the azimuth of the satellite can be properly used to estimate the characteristics of the indoor propagation channel for satellite navigation purposes.

In the second part of this column we will focus on the true Galileo E6 and L1 signal. How is it affected after penetrating the walls of a building? How does the signal power level behave and what do the spectra of the signal look like? A helicopter emitting the Galileo signal was deployed to create an opportunity to gain interesting insights to that topic.

Furthermore, in Part 2 we will investigate the properties of the building materials in greater detail. Three different test arrangements will be presented that might help us determine attenuation factors and permittivity parameters of various materials in order to develop a comprehensive transmission model.

Acknowledgement

We would like to thank Dr. Jürgen Kunisch and Jörg Pamp of IMST GmbH for their outstanding work during the field campaigns and in terms of data sampling and processing the raw data.

Additional Resources

Bach Andersen, J. et al., "The Large Office Environment – Measurement and Modeling of the Wideband Radio Channel," *The 17th Annual IEEE International Symposium on Personal, Indoor and Mobile Radio Communications (PIMRC'06)*, Helsinki, Finland, 2006

Cramer, J.M., "An Evaluation of Ultra-Wideband Propagation Channels," *Dissertation Presented to the Faculty of the Graduate School University of Southern California,* December 2000

Ganesh R., and Pahlavan, K., "Statistical Modeling and Computer Simulation of Indoor Radio Channel," *IEEE Proceedings,* Vol.138, part 1(3), pp. 153-161, June 1991

Hashemi, H., "The Indoor Radio Propagation Channel," *Proceedings of the IEEE*, Vol.18, no. 7, pp. 943-968, July 1993

Liu, C., et al., "Angle of Arrival Extended S-V Model for the 60 GHz Wireless Desktop Channel," *17th Annual IEEE International Symposium in Personal, Indoor and Mobile Radio Communications,* September 3-7, 2006

Loo, C., "A statistical Channel Model for a Land Mobile Satellite Link," *IEEE Transactions on Vehicular Technology,* Vol. 34, n.3, pp.122-127, August 1985

Lutz, E., et al., "The Land Mobile Satellite Communication Channel – Recording, Statistics and Channel Model," *IEEE Transactions on Vehicular Technology*, Vol. 40, n.2, pp. 375-386, May 1991

Molisch, A.F., et al., "IEEE 802.15.4a channel model - final report," IEEE 802.15.4a channel modeling subgroup, Texas, USA, November 2004

Nakagami, M., "The m-distribution. A general formula of intensity distribution of rapid fading", in *Statistical Methods in Radio Wave Propagation*, by W. G. Hoffman, Ed., Oxford, England, 1960

Norton, K.A. et al., "The Probability Distribution of the Amplitude of a Constant Vector Plus a Rayleigh Distributed Vector," *IRE Proceedings,* Vol. 43, pp.1354-1361, October 1955

Parkinson, B.W., "GPS Error Analysis," in *Global Positioning System: Theory and Applications.* Vol. I, B.W. Parkinson and J. J. Spilker Jr., Eds., Stanford University, USA, 1995

Saleh, A., and Valenzuela, R., "A statistical model for indoor multipath propagation," *IEEE Journal on Selected Areas of Communications,* Vol.5, no. 2, pp. 128-137, February 1987

Spencer, Q.H. et al., "Modelling the Statistical Time and Angle of Arrival Characteristics of an Indoor Multipath Channel," *IEEE Journal on selected areas in communications,* Vol. 18, no. 3, March 2000

Turin, G.L., "A Statistical Model of Urban Multipath Propagation," *IEEE Transactions on Vehicular Technology,* Vol.21, no. 1, pp. 1-9, February 1972

Authors

"Working Papers" explore the technical and scientific themes that underpin GNSS programs and applications. This regular column is coordinated by **PROF. DR.-ING. GÜNTER HEIN.** Prof. Hein is a member of the European Commission's Galileo Signal Task Force and organizer of the annual Munich Satellite Navigation Summit. He has been a full professor and director of the Institute of Geodesy and Navigation at the University of the Federal Armed Forces Munich (University FAF Munich) since 1983. In 2002, he received the United States Institute of Navigation Johannes Kepler Award for sustained and significant contributions to the development of satellite navigation. Hein received his Dipl.-Ing and Dr.-Ing. degrees in geodesy from the University of Darmstadt, Germany. Contact Prof. Hein at <Guenter.Hein@unibw-muenchen.de>.

Matteo Paonni is research associate at the Institute of Geodesy and Navigation at the University of the Federal Armed Forces Munich. He received his M.S. in Electrical Engineering from the University of Perugia, Italy. His main topics of interest are GNSS signal structure, tracking algorithms for GNSS receiver design, and indoor positioning. He is currently involved in the FEATURE (Future Satellite Navigation System Architectures) and GALIF (Interference Information System and Interference Local Isolation Methods for Satellite Navigation) ESA projects.

Victoria Kropp received her diploma in Space Geodesy from the Moscow State University of Geodesy and Cartography. She has been research associate at the Institute of Geodesy and Navigation at the University FAF Munich since 2007. Her scientific interest is statistical decision theory and indoor positioning.

Andreas Teuber is research associate at the Institute of Geodesy and Navigation at the University FAF Munich. He received his diploma in Geomatics Engineering from the University of Hannover, Germany. Currently, his main subjects of interest are indoor positioning in general and applying WLAN technology for positioning purposes in particular. IG